Scanning Electron Microscopy of the Surfaces of Ion Implanted SiC

Johan B Malherbe[1 *], NG van der Berg[1], RJ Kuhudzai[1], TT Hlatshwayo[1], TT Thabethe[1], OS Odutemowo[1], CC Theron[1], E Friedland[1], AJ Botha[2], E Wendler[3]

[1]Department of Physics, University of Pretoria, Pretoria, 0002, South Africa
[2]Laboratory for Microscopy & Microanalysis, University of Pretoria, Pretoria, 0002, South Africa
[3]Institut für Festkörperphysik, Friedrich-Schiller-Universität Jena, 07743 Jena, Germany

ABSTRACT

This paper gives a brief review of radiation damage caused by particle (ions and neutrons) bombardment in SiC at different temperatures, and its annealing, with an expanded discussion on the effects occurring on the surface. The surface effects were observed using SEM (scanning electron microscopy) with an in-lens detector and EBSD (electron backscatter diffraction). Two substrates were used, viz. single crystalline 6H-SiC wafers and polycrystalline SiC, where the majority of the crystallites were 3C-SiC. The surface modification of the SiC samples by 360 keV ion bombardment was studied at temperatures below (i.e. room temperature), just at (i.e. 350 °C), or above (i.e. 600 °C) the critical temperature for amorphization of SiC. For bombardment at a temperature at about the critical temperature an extra step, viz. post-bombardment annealing, was needed to ascertain the microstructure of bombarded layer. Another aspect investigated was the effect of annealing of samples with an ion bombardment-induced amorphous layer on a 6H-SiC substrate. SEM could detect that this layer started to crystalize at 900 °C. The resulting topography exhibited a dependence on the ion species. EBSD showed that the crystallites forming in the amorphized layer were 3C-SiC and not 6H-SiC as the substrate. The investigations also pointed out the behaviour of the epitaxial regrowth of the amorphous layer from the 6H-SiC interface.

- johan.malherbe@up.ac.za

Keywords: Nuclear materials, photovoltaic materials, SiC, SEM, radiation damage, damage annealing, implantation, ion bombardment, microstructure, topography, morphology, epitaxy

INTRODUCTION

Many of present applications and future applications of SiC is based on two of its key properties – it is one of the hardest natural materials, with a hardness of around 9.2 – 9.3 Mohs [1], and it has the ability to retain most of its properties at high temperatures – it decomposes significantly in vacuum only at about 1700°C [2]. There are two applications of SiC, where particle bombardment is a fundamental step in their operation. SiC is a wide band-gap semiconductor and can, therefore, be used in high temperature electronic devices. Doping of the SiC is usually done by ion bombardment and annealing. SiC is also used as a coating layer covering the fuel elements of the next generation of nuclear

power plants because SiC is diffusion barrier for radioactive fission products [3, 4]. This diffusion barrier property will prevent the escape of radioactive fission products into the environment during an accident in such a nuclear reactor.

For both these two applications the radiation damage properties of SiC need to be investigated. Because there is a large difference between the covalent radii of the silicon and carbon atoms, SiC has, for the common semiconductor materials, a fairly large iconicity value of 0.475 on the Garcia- Cohen scale (Phillips 0.177 and Pauling 0.11) with charge transfer to the carbon atom [5]. Because its iconicity is larger than most of the common semiconductors, it is more radiation resistant than those semiconductors. This results in potential electronic and sensor applications in a radiation environment [6, 7]. However, SiC is still mainly a covalent bonded material (88% covalency and 12% ionic). This means that it is hard to anneal radiation damaged SiC, with only very high temperatures (1500 °C and higher) being reported as successful to anneal a completely bombardment-induced amorphous SiC layer on 6H-SiC [3, 8, 9].

Most of the radiation damage and annealing studies of SiC have employed either transmission electron microscopy (TEM) or Rutherford backscattering/channeling. In this paper we report on ion bombardment-induced radiation damage of 6H-SiC and polycrystalline SiC (predominantly 3C-SiC crystallites) using SEM (scanning electron microscopy). This means that the results mainly pertain to processes occurring on the surface of these materials. We shall report on the effect of ion bombardment at room temperature and at 350 °C and 600 °C on these surfaces, and also annealing of 6H-SiC with a top amorphized layer caused by ion bombardment at room temperature.

EXPERIMENTAL

6H-SiC (from *Intrinsic Semiconductors*® and from *Pam-Xiamen*) and polycrystalline SiC – predominantly 3C-SiC crystallites - (from *Valley Design Corporation*®) samples were investigated by field emission scanning electron microscopy (FEG-SEM) employing a *Zeiss Ultra 55* instrument fitted with the usual SEM detectors and an in-lens detector. In this paper, unless specifically mentioned, mostly images taken at 2 kV in the in-lens mode are shown.

Various ions, all with an energy of 360 keV, were implanted into the SiC samples at an incidence angle of 7° to fluences of either 1×10^{16} or 2×10^{16} cm^{-2}. A dose rate of about 5×10^{12} $cm^{-2}s^{-1}$ was used. Notwithstanding this relatively low rate, temperature of the samples implanted at room temperature increased to about 50°C during the bombardment process, which will be denoted as bombarded at room temperature. To investigate the effect of substrate temperature during ion bombardment, some samples were implanted at 350°C and some at 600 °C. Some samples were vacuum annealed in a computer controlled *Webb* graphite furnace for different periods at temperatures ranging from 800 up to 1600 °C. The base pressure prior to annealing was in the range 10^{-6}-10^{-7} mbar. During annealing, the pressure sharply increased to a maximum of 5×10^{-5} mbar and then decreased to the low to middle 10^{-6} mbar range.

RESULTS AND DISCUSSION

As was mentioned in the previous section (Experimental) in this paper only SEM images taken in the in-lens mode, are shown. The in-lens detector gives SEM images showing defects present in the samples but at the expense of topographic detail, which is the *forte* of the conventional SEM detector. Crystallographic detail (an important aspect in this paper) also becomes more distinguishable in the in-lens mode. In Figure 1 a normal secondary electron SEM detector image (Figure 1 (a)) and also an in-lens SEM image (Figure 1 (b)) of the same area of a

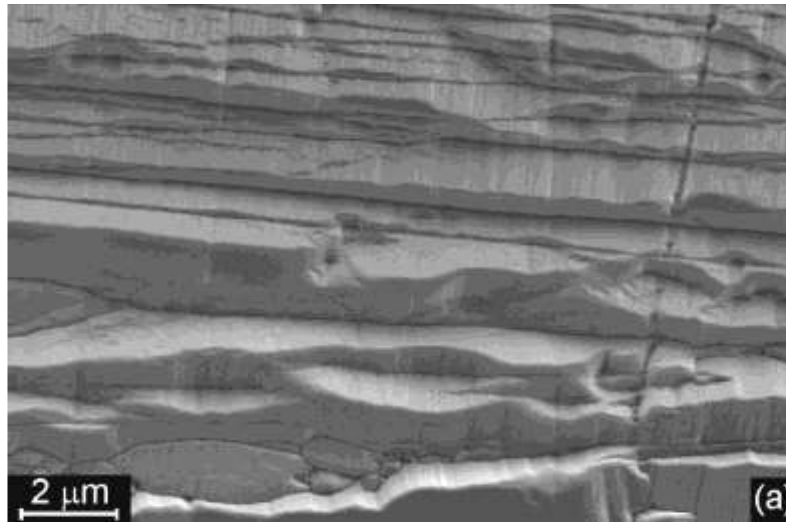

(a)

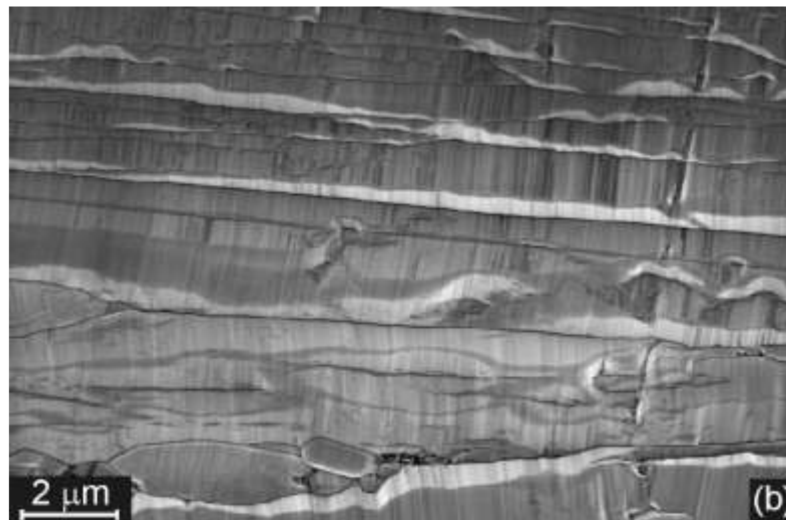

(b)

Figure 1. (a) A normal SEM image showing the facets of the different crystallites and (b) an in-lens image showing stacking faults and microstwins in the crystallites, of the same area of a polycrystalline SiC sample.

polycrystalline SiC sample are shown. In the normal SEM image the topography of the sample is clear to see. In contrast, the topography is much less pronounced in the in-lens image but many lines appear in the crystallites. These defect lines are due to twins and stacking faults, which are extremely common in SiC due to its plethora of polytypes [10]. The reason for the polytype formation in SiC (and consequent line and plane defects) lies in the very small differences in the total energy of formation between the common polytypes, viz. of the order of O(1) meV/atom, or even less [11].

Radiation damage caused by particle bombardment in SiC has recently been reviewed [3].

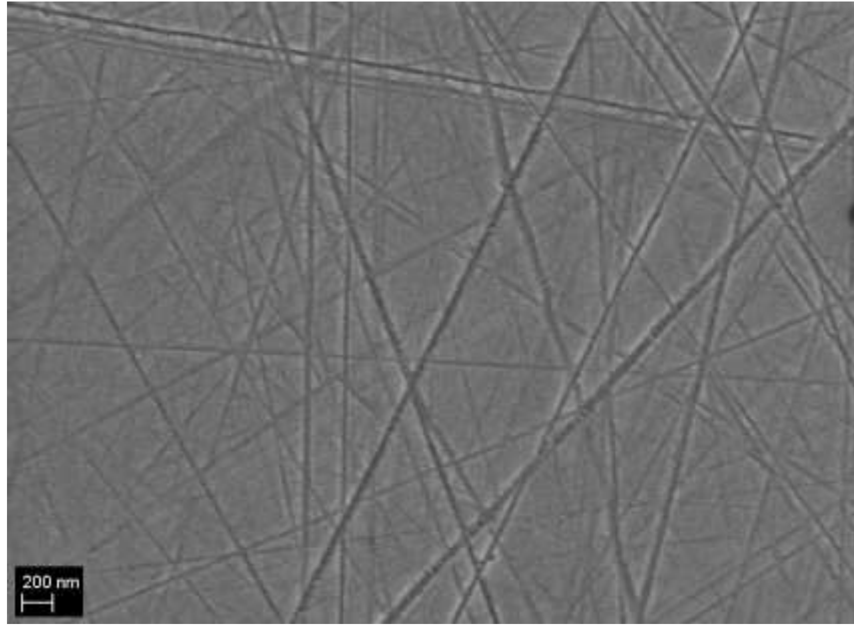

(a)

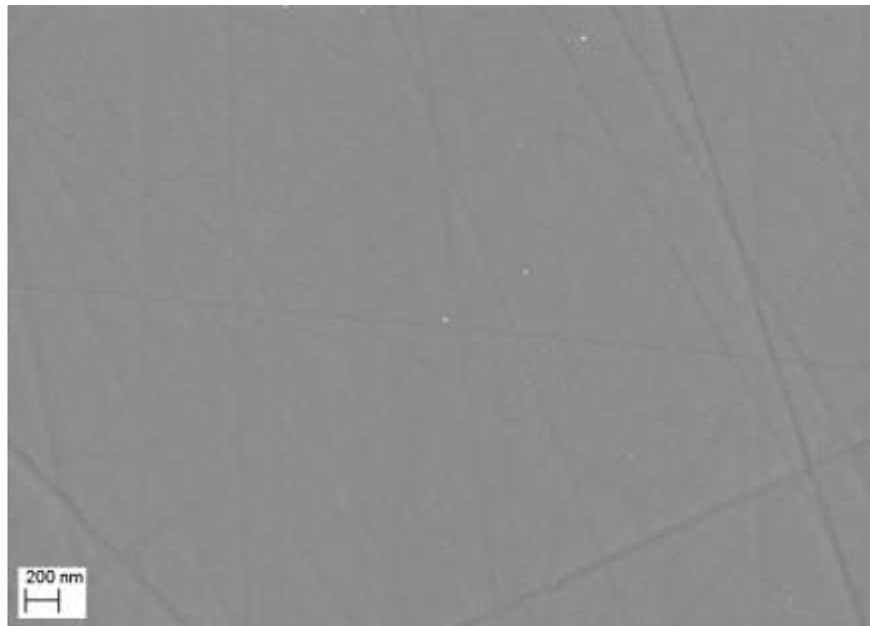

(b)

Figure 2. SEM images of (a) as-received 6H-SiC, and (b) 6H-SiC after bombardment at room temperature by 360 keV Cs^+ ions to a fluence of 2 x 10^{16} Cs^+cm^{-2}.

(a)

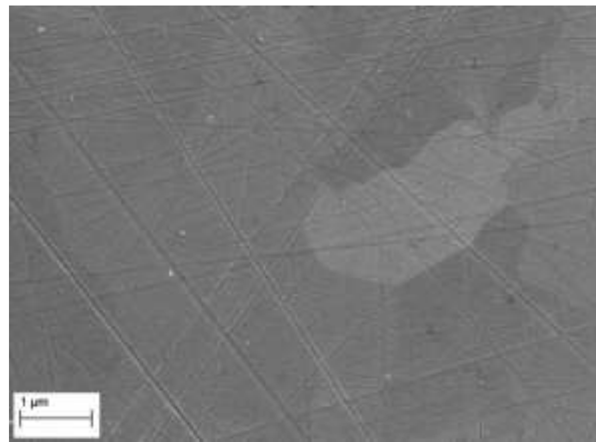

(b)

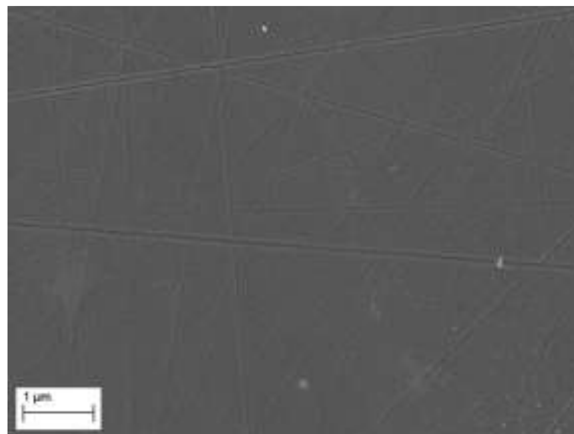

(c)

Figure 3. SEM images of polycrystalline SiC after bombardment with 360 keV Cs^+ ions to a fluence of 2 x 10^{16} Cs^+cm^{-2} at (a) room temperature, (b) 600 °C, and (b) 350 °C.

It has been reported that the radiation damage occurring in SiC at fluences below the critical fluence for amorphization is similar between ions and neutrons at the same dpa (displacements

per atom) value [12, 13]. At low temperatures and low irradiation fluences the main defects are point defects (called black spot defects due to their appearances in weak beam dark field TEM images) and small interstitial clusters in various configurations. Increasing the temperature and/or fluence result in the "black spot" defects to pass into dislocations and dislocation loops. At higher temperatures and/or fluences Frank faulted loops of the interstitial type appear with 1/3<111> Burgers vectors. Voids start to appear in the SiC at temperatures above 1000 °C and fluences above 5 dpa. At temperatures below 350 °C and with increasing fluence the damage accumulates to eventually result in amorphization according to the direct-impact/defect-stimulated model [14, 15]. At room temperature, a fluence of about 0.5 dpa is necessary for this. An aspect which makes radiation damage in SiC interesting is the fact that there is a relatively low critical temperature (approximately 350 °C) at which amorphization cannot occur [16].

The surface effect of 360 keV Cs^+ ion bombardment on 6H-SiC can be seen in Figure 2. A typical SEM image of an as-received 6H-SiC sample is shown in Figure 2(a). At high magnification, polishing marks on our optical flat 6H-SiC samples are visible. After amorphization by Cs ion bombardment, there was a reduction in the visibility and number of polishing grooves – see Figure 2(b). This is due to two effects, i.e. swelling of the SiC due to amorphization [13] and the sputter effect of the bombarding ions, which removed the more shallow grooves. For the polycrystalline SiC, ion bombardment at room temperature led to the same result. As can be seen in Figure 3(a) the number of polishing marks were significantly reduced. In addition, the individual grains were also no longer visible. The surfaces of the as-received polycrystalline SiC samples looked very similar as the one in Figure 3(b). The latter SEM image depicts the surface of a polycrystalline SiC sample after bombardment with 360 keV Cs^+ ions while the substrate was at 600 °C (i.e. above the critical temperature for amorphization). For these bombardment conditions (also true for other ions [3]) the grains and their boundaries were clearly visible indicating crystallinity. Although there was a reduction (due sputtering) in the number of polishing grooves, they were still clearly visible. When doing the ion bombardment at the critical temperature of 350 °C, the grains were longer clearly visible indicating significant damage in the surface region (Figure 3(c)). There were some indications in the image of grains but they were not conclusive enough and addition information was necessary. This was given by RBS-channeling measurements on 6H-SiC samples from the same wafers [9]. Implantation of 360 keV Cs ions at room temperature, amorphized the SiC up to a depth of about 190 nm. The crystalline structure of the 6H-SiC was retained with Cs^+ bombardment at 600 °C albeit with a large number of defects. The channelling spectrum of the samples bombarded at 350 °C showed a spectrum which practically overlapped with the random spectrum indicating a highly disordered layer. This layer is not amorphous because annealing at temperatures of 1000 °C and higher, restored the single crystal lattice [9].

As was mentioned in the Introduction, it is hard to anneal a completely bombardment-induced amorphous SiC layer on 6H-SiC and that temperatures above 1500 °C are needed [8, 9]. However, this does not mean that crystallites cannot form in amorphous SiC at much lower thermal annealing temperatures. At 900 °C crystallites on a pre-amorphized layer are visible in the SEM image shown in Figure 4. This formation of polycrystalline structures in the a-SiC layer is confirmed by a discontinuous increase in density at 900 ^{o}C [17]. Using RBS and optical methods, Wendler et al. [18] found that annealing of a-SiC even at 400 °C resulted in the layer to contain amorphized SiC regions with pockets of weakly damaged crystalline SiC. These pockets of crystalline SiC acted as seeding points for further crystalline growth as observed at 900 °C. As was shown in ref. [19] the surface crystallites, similar to the ones in Figure 4, grow in size and shape with both increasing temperature and with increasing annealing time. This solid state

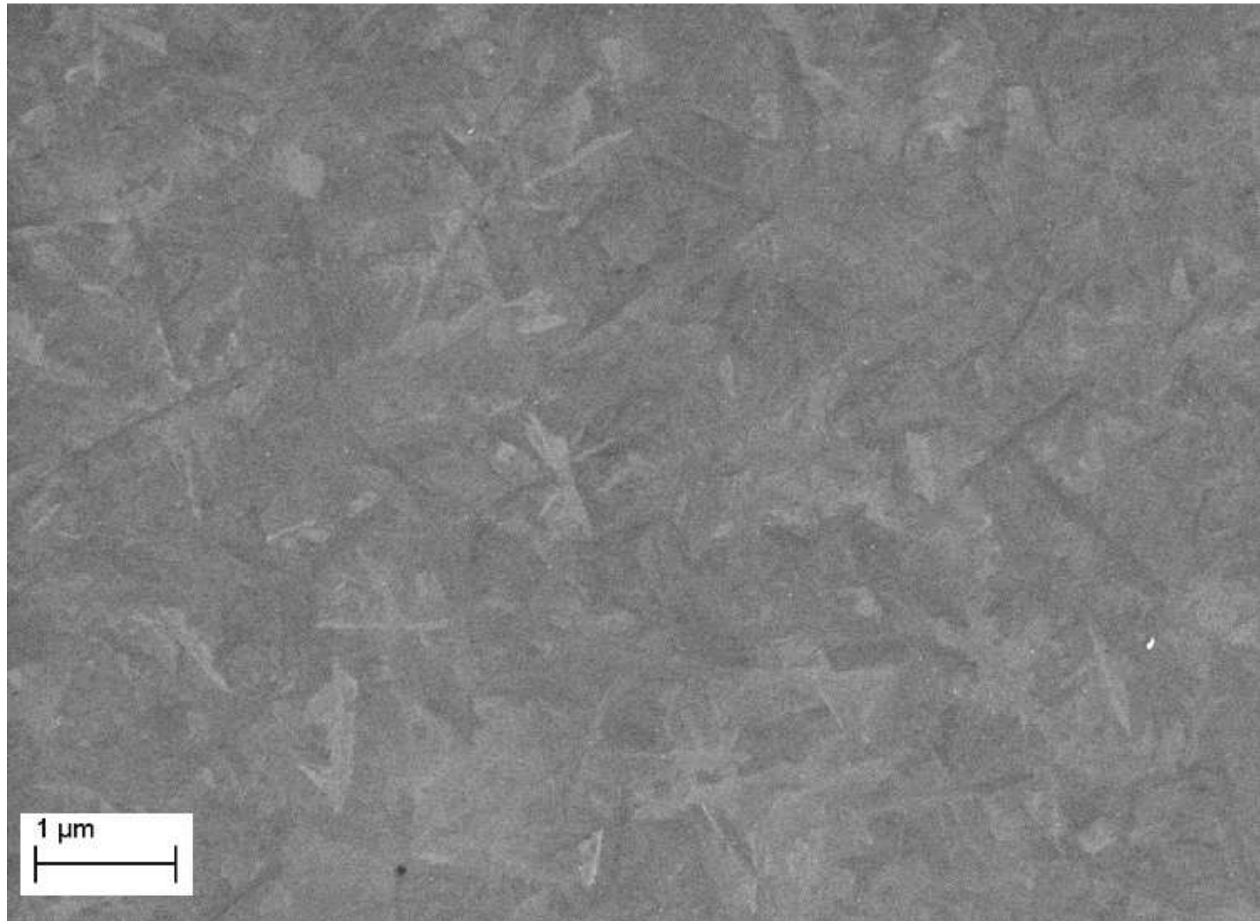

Figure 4. An in-lens SEM image showing crystallization of a 220 nm a-SiC layer on top of 6H-SiC after annealing at 900 °C for 48h. The amorphous layer resulted from bombarding a 6H-SiC wafer at room temperature with 360 keV iodine ions.

crystal growth occurs according to the flow-step model of Burton et al. [20] and Frank et al. [21]. Due to this growth process the surface becomes rough with cavities occurring at higher temperatures [19]. These two features are also visible in Figures 5 to 6. At very high annealing temperatures, i.e. 1500 °C and higher, severe thermal etching occurs, which preferentially etch certain surfaces of the crystallites away thereby reducing the crystallite sizes and eventually also the crystallites [2].

The recrystallization of the a-SiC layer on top of single crystal 6H-SiC, at the same annealing temperature and time, shows a slight dependence on the implanted atomic species [22]. As shown in Figure 5(a) a Cs implanted sample shows a fairly flat surface with small crystallites and small cavities. In contrast, the SEM image (Figure 5(b)) of an iodine implanted SiC sample shows much larger crystals. Some of these crystals (more clearly visible in Figure 6(a)) protrude above the surface with the top surface layer of these crystallites probably being one of the high energy surfaces of 3C-SiC. This growth of the crystallites in the direction of their high energy surfaces, increase the area of their lower energy surfaces, thereby minimizing the total energy of the crystallites, occurs to satisfy Wulff's law [24]. The reason for the larger crystals on the iodine implanted surface is due to the beneficiation of adding small amounts of iodine to many materials, including

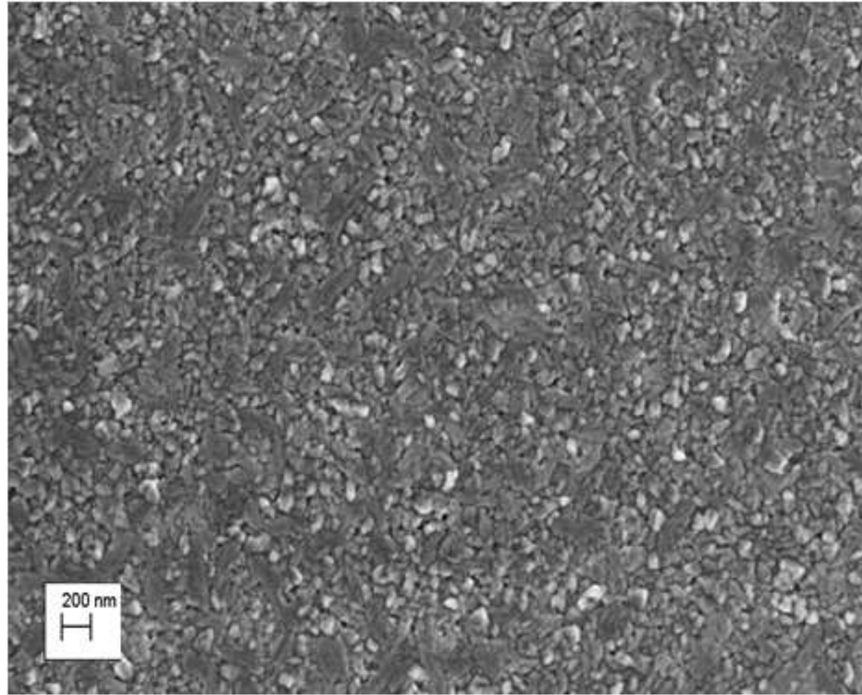

(a)

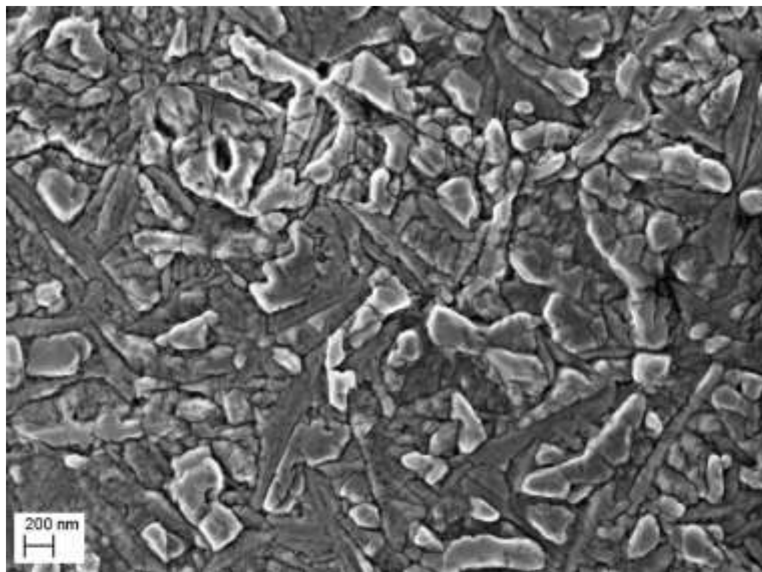

(b)

Figure 5. SEM images showing the crystallites on the originally bombardment-induced amorphous layer on top of 6H-SiC after annealing at 1200 °C for 5 h in vacuum. (a) The sample was bombarded with 360 keV Cs^+ ions. (b) A 360 keV I^+ sample.

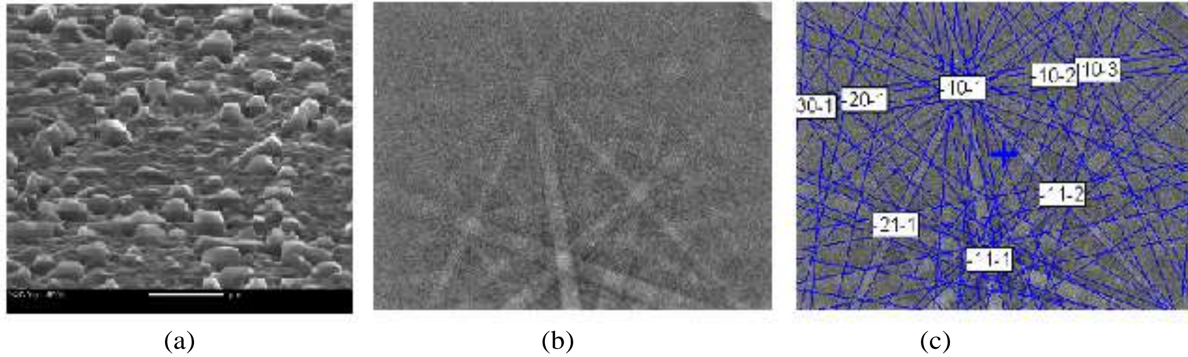

(a) (b) (c)

Figure 6. EBSD taken on a crystallite on the surface of a room temperature iodine bombarded single crystal 6H-SiC wafer and then annealed at 1400 °C for 5 h in vacuum. (a) A 20° glancing angle SEM image, taken with the normal detector, of the recrystallized surface showing several protruding crystals. Several of these crystals were analysed by EBSD. A typical EBSD analysis on one of the crystals is shown in (b) and (c). (b) A raw EBSD spectrum. (c) A computer-calculated Kikuchi-lines of the spectrum in (b).

SiC, to grow single and polycrystalline materials – see references [3] and [19] for an expanded discussion of this topic.

An interesting question is what crystal type is formed inside and on the surface during crystallization of the ion bombardment-induced a-SiC layer on top of 6H-SiC (or any other polytype) after thermal annealing. RBS channeling done in our laboratory (see for example results given in [3], [9], [24]) showed that after annealing above 1000 °C, there was gradual epitaxial regrowth taking place from the bulk 6H-SiC, independent of ion bombardment species. Solid state epitaxial growth in the damaged layer takes place until a region, nearer to the projected range of the implanted ion, is reached where the concentration of the implanted atoms starts to hinder the epitaxial growth. During the epitaxial growth process, most of these foreign atoms in the re-grown layer are also pushed towards the surface. Both these two process increase the concentration of the foreign atoms in the amorphous layer adjacent to the newly formed epitaxial layer. This leads to a situation where increasingly longer annealing times and annealing temperatures are required for the epitaxy to continue. However, the higher and longer annealing times have the detrimental effect of thermal etching of the surface and decomposition of the SiC [2] as briefly mentioned above. At the lower temperatures and annealing times considered in this paper, the amorphous region is then free to crystallize into smaller crystallites starting from the seed crystals reported by Wendler et al. [18]. Our EBSD analyses done on Ag and I implanted 6H-SiC samples showed that the surface crystallites were all 3C-SiC, not like the 6H-SiC substrate. Such a result is shown in Figure 6. This seemingly contradictory result is explained in references [3] and [22] and is based on the step-flow growth modes operating in SiC.

SUMMARY

SiC is a material with possible applications as the basis material for high temperature electronic devises and in the nuclear field. For both these two applications, the radiation damage properties of SiC need to be investigated. Traditionally, TEM (transmission electron microscopy) has been used to investigate the types of defects

introduced in SiC by particle bombardment. The disadvantage of TEM is the extensive sample preparation steps needed. Thus, it is of interest to investigate how much information can be obtained using SEM (scanning electron microscopy). A very brief review is given of radiation damage in SiC caused by particle (ion and neutron) bombardment at different temperatures.

For this study, two substrates were used, viz. single crystalline 6H-SiC wafers and polycrystalline SiC, where the majority of the crystallites were 3C-SiC. The samples were bombarded by a variety of heavy ions, all with an energy of 360 keV to a high fluence, i.e. either 1×10^{16} or 2×10^{16} cm^{-2}. High resolution SEM was mostly used in the in-lens detection mode to characterize the surfaces of the samples. An example was given to illustrate the differences using this mode in comparison to using a normal SEM detector.

Two aspects of the effect of ion bombardment on SiC surfaces were studied. The effect of the substrate temperature on the surface morphology during bombardment was investigated at three temperatures, viz. below the critical temperature for amorphization (room temperature in this case), at (or near) this temperature, i.e. 350 °C, and above the critical temperature, i.e. 600 °C. Room temperature bombardment resulted in an amorphous surface structure as detected by SEM while bombardment at 600 °C resulted in the surface to remain virtually unchanged except for some layer removal due to sputtering. The morphologies of the samples bombarded at (or near) the critical temperature looked similar to the ones done at room temperature. Thermal annealing was needed to determine whether these samples were amorphized or not by the bombardment.

The second aspect investigated was the annealing of samples with an ion bombardment-induced amorphous layer on a 6H-SiC substrate. SEM could detect that this layer started to crystalize at 900 °C. The resulting topography exhibited a dependence on the ion species. EBSD showed that the crystallites forming in the amorphized layer were 3C-SiC and not 6H-SiC as the substrate.

REFERENCES

1. Yu. Goldberg, M. Levinshtein and S. Rumyantsev, Silicon Carbide (SiC), in M. Levinshtein, S. Rumyantsev and Shur (eds.) *Properties of Advance Semiconductor Materials*, Wiley, 2001.
2. N.G. van der Berg, J.B. Malherbe, A.J. Botha and E Friedland, Appl. Surf. Sci. 258 (2012) 5561.
3. J.B. Malherbe, J. Phys. D Appl. Phys. 46 (2013) 473001.
4. J.B. Malherbe, E. Friedland, N.G. van der Berg, Nucl. Instr. Methods Phys. Res. B266 (2008) 1373.
5. Group IV Elements, IV-IV and III-V Compounds. Part b - Electronic, Transport, Optical and Other Properties Landolt-Börnstein - Group III Condensed Matter Volume 41A1b, 2002.
6. P.G. Soukiassian and H.B. Enriques, J. Phys. Condens. Matter. 16 (2004) S1611.
7. P. Soukiassian and G. Dujardin, La Recherche 321 (1999) 38.
8. C.J. McHargue and J.M. Williams, Nucl. Instrum. Meth. Phys. Res. B 80/81 (1993) 889.
9. E. Friedland, N.G. van der Berg, J.B. Malherbe, J.J. Hancke, J.R.N. Barry, E. Wendler & W. Wesch, J. Nucl. Mater. 410 (2011) 24.

10. W. Wesh, Nucl. Instrum. Meth. Phys. Res. B 116 (1996) 305.
11. S. Limpijumnong and W.R.L. Lambrecht, Phys. Rev. B 57 (1998) 12071.
12. Y. Katoh, N. Hashimoto, S. Kondo, L. Snead and A. Kohyama, J. Nucl. Mater. 351 (2006) 228.
13. L.L. Snead, T. Nozawa, Y. Katoh, T.-S. Byun,S. Kondo and D.A. Petti, J. Nucl. Mater. 371 (2007) 329.
14. W.J. Weber, Nucl. Instrum. Meth. Phys. Res. B 166-167 (2000) 98.
15. Y. Zhang, W.J. Weber, W. Jiang, A. Hallén and G. Possnert, J. Appl. Phys. 91 (2002) 6388.
16. E. Wendler, A. Heft, W. Wesch, Nucl. Instrum. Meth. Phys. Res. B 141 (1998) 105.
17. L.L. Snead and S.J. Zinkle, Nucl. Instrum. Meth. Phys. Res. B 191 (2002) 497.
18. E. Wendler, A. Heft, W, Wesch, G. Peiter and H.H. Dunken, Nucl. Instrum. Meth. Phys. Res. B 127/128 (1997) 341.
19. J.B. Malherbe, N.G. van der Berg, A.J. Botha, E. Friedland, T.T. Hlatshwayo, R.J. Kuhudzai, E. Wendler, W. Wesch, P. Chakraborty and E.F. da Silveira, Nucl. Instrum. Methods Phys. Res. B 315 (2013) 136.
20. W. K Burton, N Cabrera and F C. Frank, Phil. Trans. Roy. Soc. 243A (1931) 299.
21. F.C. Frank and J.H. van der Merwe Proc. Royal Soc. A198 (1949) 205.
22. R.J. Kuhudzai, E. Friedland, J.B. Malherbe, C. Theron, N.G. van der Berg, T.T. Hlatshwayo, E.Wendler, W. Wesch and P. Chakraborty, Nucl. Instrum. Methods Phys. Res. B 332 (2014) 251.
23. G. Wulff, Z. Krist. 34 (1901) 449.
24. T.T. Hlatshwayo, J.B. Malherbe, N.G. van der Berg, L.C. Prinsloo, A.J. Botha, E. Wendler & W.E. Wesch, Nucl. Instrum. Methods Phys. Res. B 274 (2012) 120.